Effect of flow field and geometry on the dynamic contact angle

A. V. Lukyanov[1] and Y. D. Shikhmurzaev[2]
[1]*Department of Mathematics, University of Reading, Whiteknights RG6 6AX, United Kingdom*
[2]*School of Mathematics, University of Birmingham, Birmingham B15 2TT, United Kingdom*
(Received 13 December 2006; published 22 May 2007)

A number of recent experiments suggest that, at a given wetting speed, the dynamic contact angle formed by an advancing liquid-gas interface with a solid substrate depends on the flow field and geometry near the moving contact line. In the present work, this effect is investigated in the framework of an earlier developed theory that was based on the fact that dynamic wetting is, by its very name, a process of formation of a new liquid-solid interface (newly "wetted" solid surface) and hence should be considered not as a singular problem but as a particular case from a general class of flows with forming or/and disappearing interfaces. The results demonstrate that, in the flow configuration of curtain coating, where a liquid sheet ("curtain") impinges onto a moving solid substrate, the actual dynamic contact angle indeed depends not only on the wetting speed and material constants of the contacting media, as in the so-called slip models, but also on the inlet velocity of the curtain, its height, and the angle between the falling curtain and the solid surface. In other words, for the same wetting speed the dynamic contact angle can be varied by manipulating the flow field and geometry near the moving contact line. The obtained results have important experimental implications: given that the dynamic contact angle is determined by the values of the surface tensions at the contact line and hence depends on the distributions of the surface parameters along the interfaces, which can be influenced by the flow field, one can use the overall flow conditions and the contact angle as a macroscopic multiparametric signal-response pair that probes the dynamics of the liquid-solid interface. This approach would allow one to investigate experimentally such properties of the interface as, for example, its equation of state and the rheological properties involved in the interface's response to an external torque, and would help to measure its parameters, such as the coefficient of sliding friction, the surface-tension relaxation time, and so on.

DOI: 10.1103/PhysRevE.75.051604 PACS number(s): 68.08.Bc, 68.08.De, 68.03.Cd, 83.50.Lh

I. INTRODUCTION

An important question in the physics of dynamic wetting is whether, for a given gas-liquid-solid system, the dynamic contact angle formed by an advancing free surface with a solid substrate is a mere function of the wetting speed, or its dependence on the wetting speed is just part of its dependence on the flow field near the moving contact line. In other words, is it possible to vary the contact angle at a given wetting speed by varying the flow conditions that would affect the flow field in the vicinity of the contact line? Since the influence of the flow field, obviously, cannot be accommodated in a finite or even countably infinite number of parameters, an answer to this question has fundamental implications for the modeling of free surface flows where dynamic wetting plays a role.

The assumption that the dynamic contact angle θ_d can be expressed in the form

$$\theta_d = f(U, \kappa_1, \kappa_2, \ldots), \tag{1}$$

i.e., as a function of the contact-line speed U, and material constants of the contacting media, κ_i, $i=1,2,\ldots$, motivated theoretical research aimed at funding this dependence (see [1] and Sec. 9 of [2] for reviews) as well as the appearance of a number of "master curves" used to present experimental data [3–5]. Although some discrepancies in representing the data in the form of (1) were noticed even in early experiments [1], testing of (1) and elucidating the role played by the flow field encountered formidable difficulties related to both interpretation of results and the experiments themselves. First, interpretation of the data for the contact angle obtained in experiments leaves room for speculation as to how the measured contact angle is related to the contact angle θ_d that is featured in the macroscopic fluid-mechanical models. The possibility that the two angles might be considerably different is reflected in the often used notion of an "apparent" contact angle—an auxiliary concept intended to reconcile theory and experiment by introducing an adjustable length scale interpreted as the spatial resolution of measurements [6–10]. The two angles are shown schematically in Fig. 1.

The second difficulty in investigating the influence of the flow field on the dynamic contact angle arises due to the necessity to vary the flow very near the moving contact line

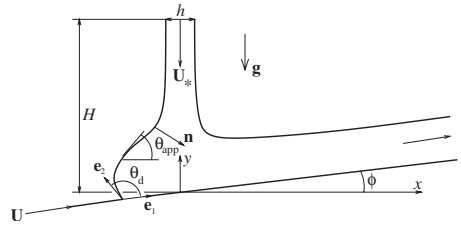

FIG. 1. Definition sketch for curtain coating. θ_d is the "actual" contact angle, i.e., the angle at which the free surface meets a solid boundary in the macroscopic fluid mechanics modeling of the flow. θ_{app} is the "apparent" contact angle formed by the tangent to the free surface at some distance from the contact line and the solid substrate; this angle is often used as an auxiliary concept to interpret experimental data.

such that the corresponding length scale becomes comparable with that associated with the specific physics of the wetting process. Such experiments would also need full-scale numerical computation of the corresponding flow to interpret the results, thus adding to the difficulties.

In the past decade, as the focus of research in dynamic wetting started to shift toward microfluidics, experimenters and theoreticians working in the area began to overcome the above problems. One flow configuration that offers considerable advantages for studying the influence of the flow field is the so-called curtain coating [11–14]. Curtain coating is a technique used in some industries [15] for depositing fluid films on solid surfaces in which a sheet of fluid impinges onto a moving solid substrate (Fig. 1). From an experimental viewpoint, curtain coating is exceptionally flexible as it allows one to manipulate the flow field by independently varying several parameters: the inlet velocity, the height of the curtain, and its initial width, as well as the angle between the falling curtain and the solid substrate. From the viewpoint of interpretation of experimental results, this flow configuration is also very convenient since it boils down to a two-dimensional steady-state problem. The presence of the second (upper) free surface makes it more difficult to solve the problem but it is via this boundary that one influences the flow field close to the wetting line.

A number of experiments [11,13,14] have shown that, for a given gas-liquid-solid system and a given contact-line speed, the measured dynamic contact angle varies considerably in response to variations in the flow field and, as a thorough numerical analysis of experiments in the framework of the so-called slip models demonstrates [16], this effect cannot be described in terms of an apparent contact angle. As was shown, the free-surface bending within the spatial resolution of the measurements (≈ 20 μm in [13]) is simply too small for the apparent contact angle to account for the observed contact-angle variations. These findings lead to the inescapable conclusion with fundamental consequences that it is the actual contact angle θ_d, i.e., the angle at which the liquid-gas interface, described as a mathematical surface, meets the solid boundary, that varies with variations in the flow field. In other words, θ_d is not a function of the wetting speed, as assumed by (1); it is a *functional* of the flow field, and hence its calculation is inseparable from finding the velocity and pressure fields in the bulk.

In the present work, we investigate the behavior of the dynamic contact angle in response to changes in the flow field at low Reynolds numbers in the framework of an earlier developed theory [17], where dynamic wetting is treated as a particular case of a flow with forming and/or disappearing interfaces. Interestingly, the theory had been published long before experimental results on the influence of the flow field on the dynamic contact angle were reported, and, as one can see from the very formulation of the problem (see the next section), treats θ_d as part of the solution to be found alongside the flow field.

The starting point of the theory [17–19] is that, as the very name suggests, dynamic wetting is a process of creating a fresh liquid-solid interface ("newly wetted solid surface"), i.e., a process of interface formation. In other words, dynamic wetting appears as a particular case in a broad class of flows with forming and/or disappearing interfaces so that the infamous moving contact-line problem can be seen as resulting from the fact that in the classical formulation of this problem all interfaces are treated as already formed, whereas one should have incorporated into the model the essential physics of formation of the liquid-solid interface, which is what dynamic wetting is all about.

As a dry solid surface is being brought into contact with the liquid, the appearing new liquid-solid interface begins to relax toward its equilibrium state. This process is characterized by some relaxation time τ, and the product $U\tau$ becomes the characteristic relaxation length over which the newly formed interface equilibrates. The notion of a contact angle is introduced into fluid mechanics via the classical Young equation [Eq. (17) below], which expresses the balance of surface tensions acting on the contact line. In the dynamic situation, the surface tensions at the contact line are out of equilibrium, and the balance of forces acting on the contact line [Eq. (16) below] indicates that the dynamic contact angle must deviate from the equilibrium one for the dynamic surface tensions to be in balance. Hence, given that θ_d is determined by the values of the surface tensions at the contact line, it depends not only on the wetting speed, which smears out the contact line, but also on the flow field near the contact line, as it is coupled with the interface formation process. Therefore, if the flow field variations caused by changes in the external conditions are characterized by a length scale comparable with $U\tau$, one should expect corresponding variations in the dynamic contact angle.

In the present paper, the theory that has been previously applied to a number of flows with forming and/or disappearing interfaces [17–23] is considered in the context of curtain coatings with the focus on the influence of the flow field and geometry on the dynamic contact angle.

II. PROBLEM FORMULATION

Consider a steady two-dimensional flow of an incompressible Newtonian liquid of constant density ρ and viscosity μ as a liquid sheet of an initial thickness h and a uniform velocity $\mathbf{U}_*$ parallel to the gravity force $\mathbf{g}$ impinges onto a moving solid substrate forming an angle ϕ with the horizontal (Fig. 1). The flow velocity $\mathbf{u}$ and pressure p in the bulk satisfy the Navier-Stokes equations

$$\nabla \cdot \mathbf{u} = 0, \quad \rho \mathbf{u} \cdot \nabla \mathbf{u} = -\nabla p + \mu \nabla^2 \mathbf{u} + \rho \mathbf{g}, \tag{2}$$

subject to the following boundary conditions.

At an *a priori* unknown free surface $f(\mathbf{r})=0$ with the inward normal $\mathbf{n}=\nabla f/|\nabla f|$, the boundary conditions are given by [17–19]

$$\mathbf{v}^s \cdot \mathbf{n} = 0, \tag{3}$$

$$-p + \mu \mathbf{n} \cdot [\nabla \mathbf{u} + (\nabla \mathbf{u})^*] \cdot \mathbf{n} = \sigma \nabla \cdot \mathbf{n}, \tag{4}$$

$$\mu \mathbf{n} \cdot [\nabla \mathbf{u} + (\nabla \mathbf{u})^*] \cdot (\mathbf{I} - \mathbf{nn}) + \nabla \sigma = 0, \tag{5}$$

$$\rho \mathbf{u} \cdot \mathbf{n} = (\rho^s - \rho^s_{1e}) \tau^{-1}, \tag{6}$$

$$\nabla \cdot (\rho^s \mathbf{v}^s) = -(\rho^s - \rho^s_{1e})\tau^{-1}, \tag{7}$$

$$(1 + 4\alpha\beta)\nabla\sigma = 4\beta(\mathbf{v}^s - \mathbf{u}) \cdot (\mathbf{I} - \mathbf{nn}), \tag{8}$$

whereas on the solid surface moving parallel to itself with velocity $\mathbf{U}$ one has

$$\mathbf{v}^s \cdot \mathbf{n} = 0, \tag{9}$$

$$\mu\mathbf{n} \cdot [\nabla\mathbf{u} + (\nabla\mathbf{u})^*] \cdot (\mathbf{I} - \mathbf{nn}) + \frac{1}{2}\nabla\sigma = \beta(\mathbf{u} - \mathbf{U}) \cdot (\mathbf{I} - \mathbf{nn}), \tag{10}$$

$$\rho\mathbf{u} \cdot \mathbf{n} = (\rho^s - \rho^s_{2e})\tau^{-1}, \tag{11}$$

$$\nabla \cdot (\rho^s \mathbf{v}^s) = -(\rho^s - \rho^s_{2e})\tau^{-1}, \tag{12}$$

$$\mathbf{v}^s \cdot (\mathbf{I} - \mathbf{nn}) = \frac{1}{2}(\mathbf{u} + \mathbf{U}) \cdot (\mathbf{I} - \mathbf{nn}) + \alpha\nabla\sigma. \tag{13}$$

Here σ is the surface tension in the interfacial layer, which is modeled as a two-dimensional surface phase; ρ^s is the surface density in this phase (mass per unit area), and $\mathbf{v}^s$ is the velocity with which it is transported along the interface; α, β, γ, τ, and ρ^s_{ie} $(i=1,2)$ are phenomenological material constants; $\mathbf{I}$ is the metric tensor; the tensor $(\mathbf{I}-\mathbf{nn})$ singles out the tangential projection of a vector so that, for example, $\mathbf{u}\cdot(\mathbf{I}-\mathbf{nn})=\mathbf{u}_{\|}$; an asterisk marking a second-rank tensor indicates its transposition.

Conditions (3)–(8) have been obtained using methods of irreversible thermodynamics so that here we will only briefly recapitulate their meaning with more detail available in the cited works. On the free surface, in addition to the usual conditions on the normal and tangential stresses (4) and (5), the model takes into account mass exchange between the bulk and the surface phase (6) and (7) that takes place when the surface density ρ^s deviates from its equilibrium value ρ^s_{1e}. Similar to (6) and (7), conditions (11) and (12) describe mass exchange between the bulk and the liquid-solid interface. More importantly, the tangential components of the velocity in the surface phase $\mathbf{v}^s$, the bulk velocity evaluated on the *liquid-facing* side of interfaces $\mathbf{u}$, and the velocity of the solid substrate $\mathbf{U}$ are, in the general case, all different due to the torques acting on the surface phase. The conditions relating these components are given by (8) on the free surface and (10) and (13) on the solid boundary. These equations are a bit less self-explanatory than the other ones so that a brief comment seems appropriate.

Both the liquid-gas and the liquid-solid interfaces represent different states of essentially the same physical object—a thin layer of liquid between two bulk phases subject to asymmetric action of intermolecular forces from these phases. In addition to these forces which, from a macroscopic viewpoint, determine the equilibrium parameters of the interface (ρ^s_{1e} and ρ^s_{2e} in the above equations), the bulk phases exert macroscopic tangential forces on the interface. The liquid-solid interface experiences the shear stress from the liquid together with the drag force from the solid, and the difference between the tangential velocities on the opposite sides of the interface results from, and is proportional to, the torque produced by these forces. This is a general statement that holds for different dissipative systems [24]. On the other hand, however, due to the negligible inertia of the interface, the total force on its elements resulting from the action of shear stress, the drag force, and the surface tension gradient is equal to zero. Then, by eliminating the drag force from the equation expressing the above statements, one arrives at the generalized Navier condition (10). It should be emphasized that, unlike some *ad hoc* generalizations of the Navier conditions proposed recently [25], condition (10) is *local* and *universal* in the sense that, like all boundary conditions of classical fluid mechanics, it involves only the variables at the point where it is applied and is not specific to the moving contact-line problem.

It should also be noted that $\mathbf{u}$ that is featured in (10), as well as in all other boundary conditions, is the velocity on the liquid-facing side of the interface. It is assumed that on the solid-facing side of the interface the velocity is equal to that of the solid, so that there is no actual slippage of the liquid on solid that would have been detected, for example, by molecular dynamics simulations. The difference between the tangential components of $\mathbf{u}$ (i.e., the velocity on the liquid-facing side of the interface) and $\mathbf{U}$ can be referred to as "apparent slip" that appears only in the macroscopic (hydrodynamic) modeling of interfaces.

Condition (13) has the form of a Darcy law in the interfacial layer expressing the velocity $\mathbf{v}^s$ in this layer via the velocities on its opposite sides and the surface tension gradient. The latter is analogous to the (negative) pressure gradient acting in a Couette-Poiseuille flow in a channel.

Finally, condition (8) can be understood as follows. If one applies (10) and (13) to the liquid-gas interface and eliminates $\mathbf{U}$ (which in this case would be the velocity on the gas-facing side of the interface), then, after making use of the force balance condition (5), one arrives at (8).

The meaning of the phenomenological material constants involved in (3)–(13) follows from the physical meaning of these equations. The constants α and β describe the response of the velocity distribution across an interface to the surface tension gradient and the external torque, respectively. The analysis of experiments, e.g., [20,26], shows that these constants, as well as the relaxation time τ, depend on the fluid's viscosity: $\alpha \propto \mu^{-1}$, $\beta \propto \mu$, $\tau \propto \mu$. The experimentally determined estimates for these constants for some fluids can be found in [19,26].

The equation of state in the surface phase that is needed to close the set of equations (3)–(13) for the surface variables is taken in a barotropic form linking the surface tension σ with the surface density:

$$\sigma = \gamma(\rho^s_{(0)} - \rho^s), \tag{14}$$

where γ and $\rho^s_{(0)}$ are phenomenological constants. This equation is the simplest one accounting for the fact that the surface tension decreases from its equilibrium value $\sigma_{1e} = \sigma(\rho^s_{1e})$ in the free surface to that in the liquid-solid interface, $\sigma_{2e} = \sigma(\rho^s_{2e})$, when the interfacial layer becomes more compressed (or, more generally, less rarified) due to the ac-

tion of intermolecular forces from the bulk phases that determine the equilibrium values of ρ^s. From the modeling viewpoint, an equation of state is always an assumption to be validated experimentally. The model with the simplest linear barotropic closure (14) that we are studying here has been shown to be in very good agreement with experiments available in the literature [2,17,19], and so far there are no experimental indications pointing to the necessity of replacing (14) with a more general equation of state or the form such an equation might have.

Distributions of the surface parameters along the interfaces are linked at the contact line via the mass and momentum balance conditions:

$$\rho_1^s \mathbf{v}_1^s \cdot \mathbf{e}_1 + \rho_2^s \mathbf{v}_2^s \cdot \mathbf{e}_2 = 0, \tag{15}$$

$$\sigma_1 \cos\theta_d = \sigma_3 - \sigma_2, \tag{16}$$

where the subscripts 1 and 2 refer to the limiting values as one approaches the contact line along the free surface and the solid-liquid interface, respectively; $\mathbf{e}_1$ and $\mathbf{e}_2$ are unit normals to the contact line directed along the appropriate interfaces (Fig. 1); σ_3 is the surface tension of the gas-solid interface, which for a perfect system, i.e., in the absence of adsorbed molecules of liquid and gas, is equal to zero. For the cosine of the dynamic contact angle θ_d one has $\cos\theta_d = \mathbf{e}_1 \cdot \mathbf{e}_2$. In equilibrium, the dynamic contact angle is related to the static one θ_s via the classical Young equation

$$\sigma_{1e} \cos\theta_s = \sigma_3 - \sigma_{2e} \tag{17}$$

that links the material constants σ_{1e}, σ_{2e}, and σ_3 [or, alternatively, after using (14), ρ_{1e}^s, ρ_{2e}^s, $\rho_{(0)}^s$, γ, and σ_3] and hence allows one to replace one of them with θ_s, which is a quantity relatively easy to measure in experiments.

The boundary conditions (3)–(16) describe the surface phases and the contact line as elements of a fluid-mechanical model.

In order to model curtain coating, we need to formulate additional boundary conditions specifying this particular flow. After introducing a Cartesian coordinate system as shown in Fig. 1, for the bulk flow one can set the inlet velocity and thickness of a falling liquid sheet:

$$\mathbf{u} = \mathbf{U}_* \quad \text{for } -h/2 \leqslant x \leqslant h/2, \quad y = H, \tag{18}$$

where the inlet velocity $\mathbf{U}_*$ is assumed to be uniform and has only the y component, together with boundary conditions far downstream, which we will set in a soft form:

$$\frac{\partial \mathbf{u}(x',y')}{\partial x'} \to 0 \quad \text{as } x' \to +\infty, \quad 0 < y' < \tilde{h}, \tag{19}$$

where $x' = x\cos\phi + y\sin\phi$, $y' = -x\sin\phi + y\cos\phi$, and $\tilde{h}$ is to be determined. For the surface variables we will assume that at the top of the curtain the interfaces are in equilibrium, i.e.,

$$\rho^s = \rho_{1e}^s, \quad \mathbf{v}^s = \mathbf{u} \quad \text{for } x = \pm h/2, \quad y = H, \tag{20}$$

and that far downstream along the solid surface the liquid-solid interface tends to its equilibrium state:

$$\rho^s \to \rho_{2e}^s \quad (x \to +\infty, \quad y = x\tan\phi). \tag{21}$$

Equations (2)–(16) and (18)–(21) fully specify the problem.

III. EFFECT OF THE FLOW FIELD AND GEOMETRY ON THE DYNAMIC CONTACT ANGLE

After nondimensionalizing (2)–(16) and (18)–(21) using U, h, $\mu U h^{-1}$, σ_{1e}, and $\rho_{(0)}^s$ as scales for velocity, length, pressure, surface tension, and surface density, respectively, one arrives at the problem whose solution is specified by dimensionless similarity parameters that can be divided into the following three groups. First is the Reynolds and Froude numbers, $\mathrm{Re} = \rho U h/\mu$, $\mathrm{Fr} = U^2/(gh)$, i.e., the parameters that characterize the bulk flow. In microfluidics, one almost invariably has creeping flows with negligible inertia. For the problem we are considering $h \sim 2$–4 μm, $U \sim 1$ cm s^{-1}, $\mu/\rho \sim 60$ cSt [1 centistokes (cSt) $= 10^{-2}$ cm^2/s] giving $\mathrm{Re} \leqslant 10^{-3}$, so that the convective term in (2) can be neglected. Although the ratio Re/Fr is also small ($\leqslant 4 \times 10^{-4}$ for our flow conditions), in the computations it is convenient to keep the body force term in (2) as a stabilizing factor for the film far downstream of the solid substrate.

The second group of dimensionless parameters includes, first, the similarity groups formed by the material constants characterizing the contacting media, θ_s, $\bar{\rho}_{1e}^s = \rho_{1e}^s/\rho_{(0)}^s$, $A = \alpha\beta$, and $\bar{\sigma}_3 = \sigma_3/\sigma_{1e}$, and, second, the parameters depending on material constants and the contact-line speed only: $\mathrm{Ca} = \mu U/\sigma_{1e}$, $Q = \rho_{(0)}^s/(\rho U \tau)$, $\bar{\beta} = \beta U h/\sigma_{1e}$, and $\epsilon = U\tau/h$. All these parameters remain constant for a given set of materials and a given contact-line speed.

Finally, we have three parameters $\bar{U}_* = U_*/U$, $\bar{H} = H/h$, and ϕ whose variation, for a given contact-line speed and given materials of the system, leads to variation in the flow field and geometry in the vicinity of the contact line. We will consider the influence of these parameters on the dynamic contact angle θ_d as a key to the effect that came to be known as "hydrodynamic assist of dynamic wetting" [11].

In order to narrow down the region in the parameter space to be investigated in what follows, we will take the range of dimensional material constants corresponding to water-glycerol solutions previously studied using the present model [26].

The main difficulty in computing the solution arises due to the nature of the physical effect we are trying to capture. The formulation (2)–(16) and (18)–(21) introduces the dynamic contact angle θ_d via the Young equation (16) and hence makes it part of the solution dependent on the dynamic values of the surface tensions at the contact line, which, in their turn, are determined by the distributions of the surface parameters along the interfaces. These distributions are linked with the bulk stress and velocity evaluated at the interfaces via (5), (6), (8), (10), (11), and (13) so that θ_d becomes a functional of the flow field. On the other hand, however, the value of θ_d is a boundary condition for (4) which determines the free-surface profile and hence the shape of the flow domain, thus giving a feedback to the flow field. This interdependence of the bulk, interfacial, and

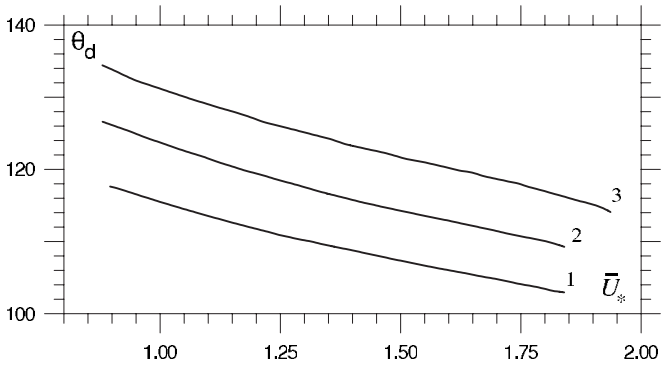

FIG. 2. Dependence of the dynamic contact angle on the dimensionless inlet velocity for $\bar{H}=10$, $\phi=0°$, and different contact-line speeds. Curve 1, Ca=0.02, $Q=0.04$, $\bar{\beta}=20$, $\epsilon=0.025$. Curves 2 and 3 are obtained by increasing the contact-line speed by 12.5% and 25%, respectively; $\theta_s=60°$, $\bar{\rho}^s_{1e}=0.8$, $A=1$, $\bar{\sigma}_3=0$ for all curves.

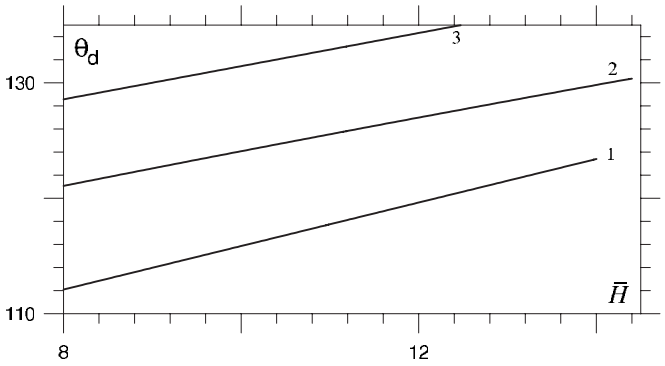

FIG. 3. Dependence of the dynamic contact angle on the dimensionless height of the curtain for $\bar{U}_*=1$, $\phi=0°$, and different contact-line speeds with other parameters being the same as in Fig. 2.

contact-line characteristics makes even a numerical solution of the problem (2)–(16) and (18)–(21) a formidable task since, in addition to the known difficulties of computing free-boundary flows [27], one has to pay particular attention to the accuracy with which the distributions of the surface parameters along the interfaces are resolved. It is their values at the contact line that, via the contact angle, have a global effect on the shape of the computational domain, and hence on the bulk flow, which, in its turn, affects the surface distributions. As a result, every element of the model appears to be sensitive to the accuracy with which all other elements are computed, and the control of computational accuracy becomes a complex task.

The problem was solved numerically using a combined boundary integral equation–finite element algorithm that has the capacity to resolve the distributions of the surface parameters in the immediate vicinity of the contact line and handle the contact angle itself with sufficient accuracy (the finite element part of the method) and, at the same time, allows one to describe the creeping free-surface flow away from the contact line in an efficient and flexible way (the boundary integral equation part). The details of the algorithm can be found elsewhere [28].

Figures 2–4 summarize the effect on θ_d of the parameters controlling the flow field. As one can see, for a given contact-line speed, the parameters $\bar{U}_*$, $\bar{H}$, and ϕ do have a significant effect on the dynamic contact angle. An alternative way of interpreting these figures is that, for the same materials of the system, the dependence of θ_d on the capillary number (i.e., the dimensionless contact-line speed) is different for different flow geometries, which, in our case, are specified by $\bar{U}_*$, $\bar{H}$, and ϕ. This nonuniqueness of the velocity dependence of the dynamic contact angle was indeed observed in experiments [13].

IV. MECHANISM OF THE EFFECT

As mention earlier, all elements in the model are interdependent and therefore, strictly speaking, it would be incorrect to single out direct causal links between any two of them in terms of "causes" and "consequences." However, for relatively low capillary numbers, as in the flow we are considering here, one can arrive at a qualitative understanding of the mechanism by which the flow field influences the dynamic contact angle. For this purpose we will, first, examine the distributions of the surface variables ρ^s and v^s corresponding to different points along one of the curves given in Fig. 2. These distributions are shown in Fig. 5.

As the plots of the surface density show (Fig. 5), on the free surface the deviations of ρ^s from its equilibrium value, being proportional to Ca, are small, and hence the variations in the mass flux into the contact line, $-\rho^s_1 \mathbf{v}^s_1 \cdot \mathbf{e}_1$, which is featured in (15), are determined primarily by the variations of v^s_1. The value of v^s_1 increases as the inlet velocity $\bar{U}_*$ goes up, thus increasing the mass flux into the forming liquid-solid interface. In the process of dynamic wetting, the liquid-solid interface near the contact line is always "starving" ($\rho^s < \rho^s_{2e}$) since it begins to form out of the liquid-gas interface that moves into the contact line with velocity lower than the velocity U of the solid substrate that drags the (solid-facing side of the) liquid-solid interface out of the contact line. The surface density carried by v^s_1 is also always lower than ρ^s_{2e}. Therefore, an increase in v^s_1 due to an increase in $\bar{U}_*$ reduces starvation of the liquid-solid interface, i.e., the difference be-

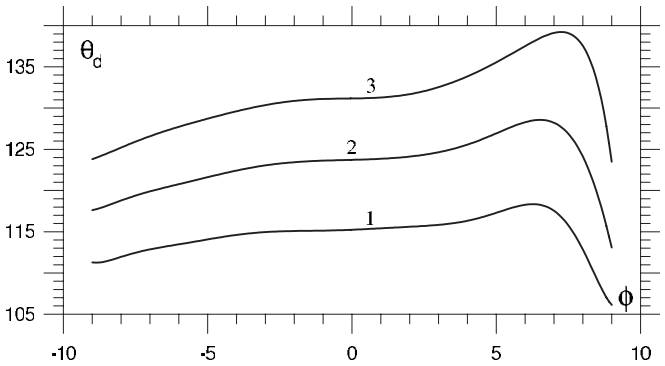

FIG. 4. Dependence of the dynamic contact angle on the angle of inclination of the solid substrate for $\bar{U}_*=1$, $\bar{H}=10$, and different contact-line speeds as in Fig. 2.

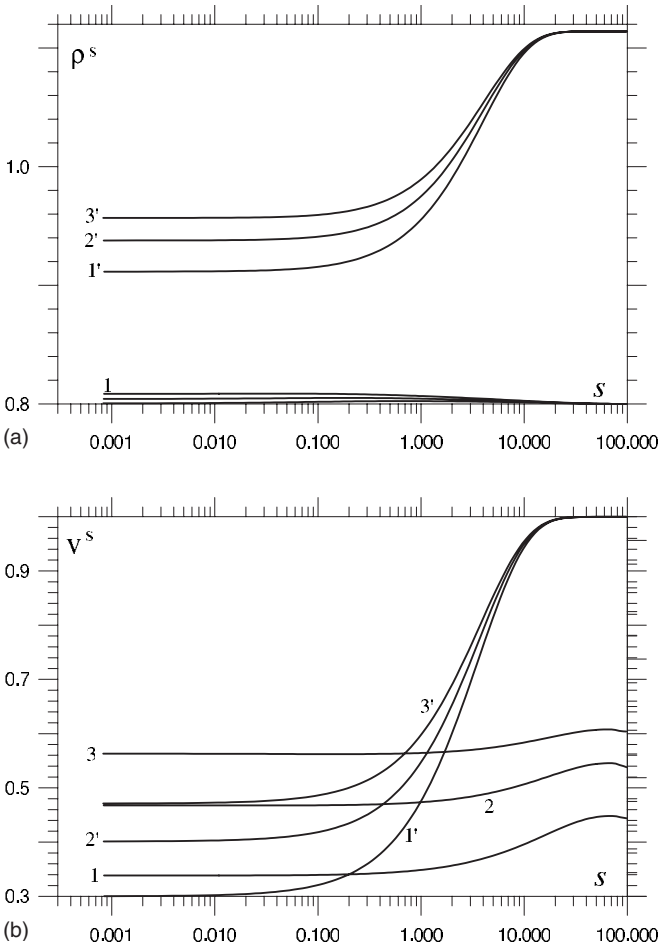

FIG. 5. Distributions of the surface parameters along the free surface and the liquid-solid interface (marked with a prime) at different points along curve 1 of Fig. 2. $\bar{U}_*$=(1) 0.91, (2) 1.38, and (3) 1.82. The distance s from the contact line is scaled with $U\tau$; the data point corresponding to s=0 and a few neighboring points are taken out. It is important to note that the actual distance over which the surface parameters relax to their equilibrium values is greater, often considerably, than the formally defined surface-tension relaxation length $U\tau$.

tween its surface density at the contact line, ρ_2^s, and far away from it, ρ_{2e}^s (see Fig. 5). Then, according to the Young equation (16), this leads to a decrease in the value of the dynamic contact angle, which acts as a mechanism balancing the tangential forces exerted on the contact line by the interfaces. In other words, an increase in the mass flux into the contact line from the free surface brings the surface density of the liquid-solid interface at the contact line closer to its equilibrium value, and hence drives θ_d closer to θ_s.

The above explanation also makes clear why an increase in the dimensionless curtain height $\bar{H}$ increases the dynamic contact angle (Fig. 3): as $\bar{H}$ goes up, the effect of the inlet velocity on the flow near the contact line diminishes, leading to lower mass flux into the contact line, thus increasing starvation of the liquid-solid interface and consequently the dynamic contact angle. It should be emphasized that, unlike curtain coating in macroscopic hydrodynamics, which is driven by gravity so that the impingement velocity increases

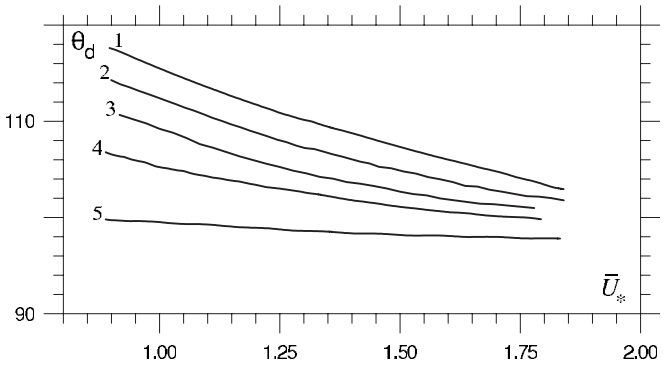

FIG. 6. Dependence of the dynamic contact angle on the inlet velocity for different scales of the system (different h, the same $\bar{H}$). Curve 1 is identical to curve 1 in Fig. 2; (2) ϵ=0.02, $\bar{\beta}$=25; (3) ϵ=0.015, $\bar{\beta}$=33; (4) ϵ=0.01, $\bar{\beta}$=50; (5) ϵ=0.005, $\bar{\beta}$=100.

with the curtain height, in the low-Reynolds-number regime considered here $\mathbf{v}_1^s$ is determined by the inlet velocity U_*, with gravity playing a negligible role, so that an increase in H reduces $\mathbf{v}_1^s$ and hence increases the contact angle.

Thus, for small capillary numbers the mechanism of the influence of the flow field on the dynamic contact angle is relatively transparent: the contact angle responds to the influence of the flow conditions on the tangential velocity of the free surface near the contact line that controls the supply of mass into the contact line required for the formation of the liquid-solid interface. An increase in v^s reduces starvation of the liquid-solid interface and hence the contact angle, thus, using the terminology of [11], assisting dynamic wetting.

A key requirement for the above hydrodynamic assist to take place is that the length scale characterizing variations in the flow field must be comparable with the surface-tension relaxation length. In our model, this condition is reflected in the parameter ϵ, which is exactly the ratio of the two lengths. Computations show (Fig. 6) that, if the system as a whole is magnified (i.e., h and H proportionally increase), the effect of hydrodynamic assist diminishes and eventually disappears. (Formally, for a given system, the magnitude of the effect can be attributed to one parameter ϵ, by eliminating h

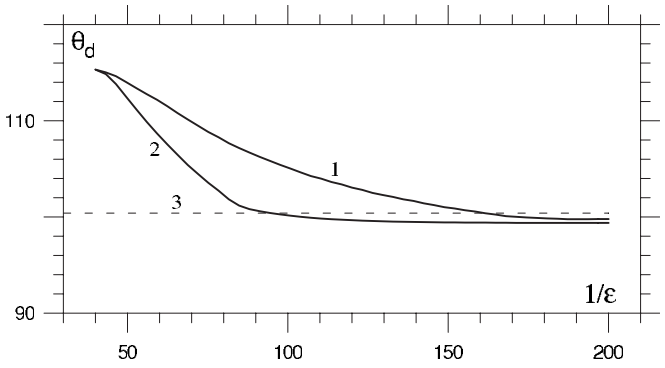

FIG. 7. Dependence of the dynamic contact angle on the (inverse) dimensionless relaxation length. Curve 1, constant $\bar{H}$ (=10); curve 2, constant H. Ca=0.02, $\bar{U}_*$=1, ϕ=0 for both curves. The dashed line (3) corresponds to the asymptotic solution for low capillary numbers [17].

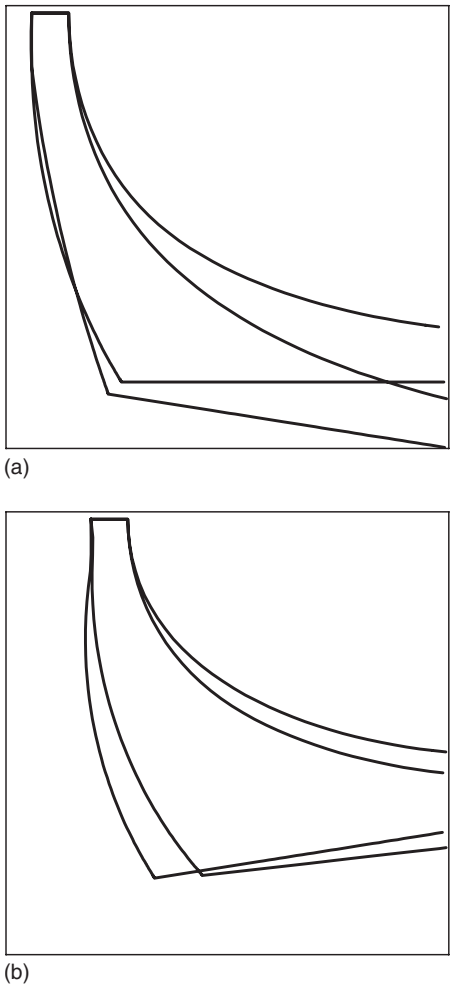

FIG. 8. Curtain profiles for different points along curve 1 in Fig. 4: $\phi=-9°$ and 0° (a) and 6.5° and 9° (b).

from $\bar{\beta}$, i.e., replacing it with $\epsilon^{-1}\bar{\bar{\beta}}$, where $\bar{\bar{\beta}}=\beta\tau U^2/\sigma_{1e}$ is proportional to V^2 introduced in [17].)

In order to understand the origin of complexity of the contact-angle dependence on ϕ shown in Fig. 4, it is instructive to look at the role played by the upper free surface. As shown in Fig. 7, the dynamic contact angle is reduced as this surface is moved away from the contact line, either by increasing h and H proportionally or by increasing h and keeping H constant. Then one has to conclude that, perhaps counterintuitively, the constraint on the flow due to the presence of the free surface slows down the flow near the contact line and hence, by reducing v_1^s, increases the dynamic contact angle. It is the removal of this surface that assists dynamic wetting. (It is worth emphasizing once again that here we are dealing with flows at zero Reynolds and small capillary numbers.)

Figure 7 shows that, as $\epsilon\to 0$, the dynamic contact angle tends asymptotically to a constant value slightly below the one resulting from the leading-order asymptotic solution as $\mathrm{Ca}\to 0$ [13,17]. The reason for this effect is clear: although in the present study the capillary number is (numerically) small, no asymptotic simplifications based on the smallness of Ca have been used and the computed surface density on

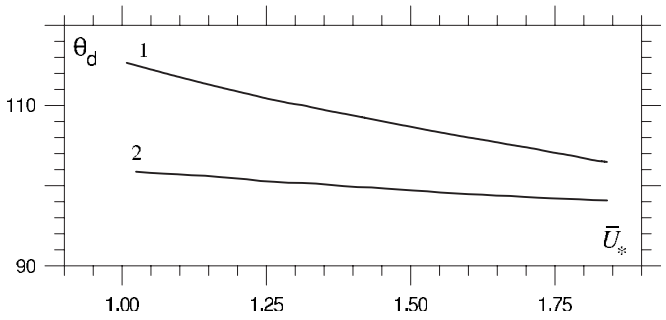

FIG. 9. Dependence of the dynamic contact angle on the inlet velocity for different values of $\bar{\rho}_{1e}^s$. Curve 1 is identical to curve 1 in Fig. 2 ($\bar{\rho}_{1e}^s=0.8$); curve 2, $\bar{\rho}_{1e}^s=0.6$.

the free surface (Fig. 5) deviates from ρ_{1e}^s as one approaches the contact line, whereas in the leading-order asymptotic solution in Ca as $\mathrm{Ca}\to 0$ one obviously has $\rho^s\equiv\rho_{1e}^s$. The slight increase in ρ^s as one approaches the contact line leads to a slight reduction in σ [Eq. (14)] and hence to a lower value of θ_d needed to balance the forces at the contact line.

Thus, the dependence of θ_d on ϕ in Fig. 4 results from the interplay of two factors: the slowing down of the flow as its direction changes by a larger angle due to the inclination of the solid substrate (hence an increase in θ_d) and the reduction of the influence of the upper free surface as it becomes positioned further away from the contact line (hence a reduction in θ_d). Typical profiles of the free surface near the contact line corresponding to one of the curves in Fig. 4 are shown in Fig. 8.

A material-related factor that determines the magnitude of the effect of hydrodynamic assist is $1-\bar{\rho}_{1e}^s=\sigma_{1e}/(\gamma\rho_{(0)}^s)$,

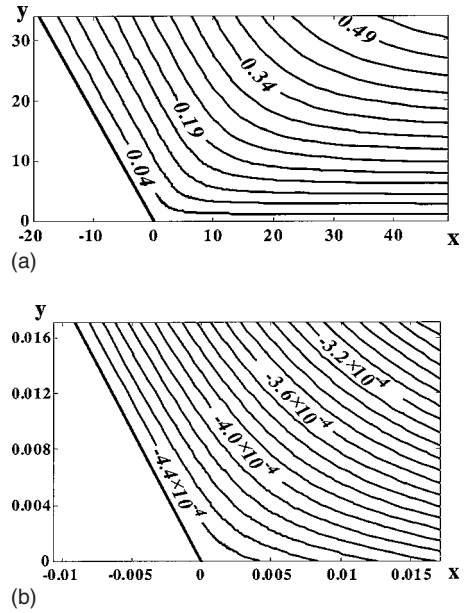

FIG. 10. Typical pattern of streamlines with the distances measured in relaxation lengths $U\tau$. Left: the general pattern where, unlike the slip models analyzed in [18], the region near the contact line is associated with a more intensive flow than further afield. Right: magnified view of the flow near the contact line showing adsorption of the fluid into the forming liquid-solid interface.

which is essentially a measure of the influence of the intermolecular forces acting from the bulk phases on the interfacial layer's density. The closer $\bar{\rho}_{1e}^{s}$ is to 1, the smaller is the possible amplitude of variation of the surface density, $\bar{\rho}_{2e}^{s} - \bar{\rho}_{1e}^{s}$, and hence the stronger becomes the influence of the changes in v^s that result in variations of θ_d. This sensitivity of θ_d to $1-\bar{\rho}_{1e}^{s}$ illustrated in Fig. 9 could be used in experiments to investigate the equation of state in the surface phase.

V. FLOW FIELD

The flow near the moving contact line has some interesting features. On a length scale large compared with the surface-tension relaxation length (Fig. 10, left) the streamlines form an expected pattern. Importantly, the flow is more intensive near the contact line than further afield, as is indeed observed in experiments [12], whereas the slip models make the region near the contact line a stagnation zone [18].

After zooming in to the contact line and considering the flow on a length scale comparable with $U\tau$ (Fig. 10, right), one can see that, in accordance with (11), the starving liquid-solid interface adsorbs the fluid so that the liquid-solid interface is no longer a streamline. According to (6) and the surface density distributions shown in Fig. 5, one also has desorption from the liquid-gas interface, though this effect is too small to be visualized here. Thus, the numerical solution confirms the local asymptotic analysis given in [18].

VI. CONCLUSION

It has been shown that the interface formation theory predicts that in the process of dynamic wetting, for a given contact-line speed and materials of the system, the actual dynamic contact angle θ_d depends on the flow field and geometry in the vicinity of the moving contact line. This effect becomes more pronounced as the ratio of the surface-tension relaxation length $U\tau$ to the length scale characterizing variations in the (Stokes) flow near the contact line due to changes in the flow conditions increases. In the case of relatively low capillary numbers, the mechanism of the dependence of the dynamic contact angle on the flow field can be explained in terms of the influence of the flow on the tangential velocity of the free surface, which determines the mass flux into the contact line that goes into the formation of a fresh liquid-solid interface. The magnitude of the response of the contact angle to the changes in the flow field depends on the material constants specifying the equation of state in the surface phase.

[1] V. E. B. Dussan, Annu. Rev. Fluid Mech. **11**, 371 (1979).
[2] Y. D. Shikhmurzaev, J. Fluid Mech. **334**, 211 (1997).
[3] R. Hoffman, J. Colloid Interface Sci. **50**, 228 (1975).
[4] T. S. Jiang, S. G. Oh, and J. C. Slattery, J. Colloid Interface Sci. **69**, 74 (1979).
[5] M. Bracke, F. De Voeght, and P. Joos, Prog. Colloid Polym. Sci. **79**, 142 (1989).
[6] V. E. B. Dussan, J. Fluid Mech. **77**, 665 (1976).
[7] O. V. Voinov, Fluid Dyn. **11**, 714 (1976).
[8] L. M. Hocking, J. Fluid Mech. **79** 209 (1977).
[9] L. M. Hocking and A. D. Rivers, J. Fluid Mech. **121**, 425 (1982).
[10] R. G. Cox, J. Fluid Mech. **168**, 169 (1986).
[11] T. D. Blake, A. Clarke, and K. J. Ruschak, AIChE J. **40**, 229 (1994).
[12] A. Clarke, Chem. Eng. Sci. **50**, 2397 (1995).
[13] T. D. Blake, M. Bracke, and Y. D. Shikhmurzaev, Phys. Fluids **11**, 1995 (1999).
[14] A. Clarke and E. Stattersfield, Phys. Fluids **18**, 048106 (2006).
[15] *Liquid Film Coating*, edited by S. F. Kistler and P. M. Schweizer (Chapman & Hall, London, 1997).
[16] M. C. T. Wilson, J. L. Summers, Y. D. Shikhmurzaev, A. Clarke, and T. D. Blake, Phys. Rev. E **73**, 041606 (2006).
[17] Y. D. Shikhmurzaev, Int. J. Multiphase Flow **19**, 589 (1993).
[18] Y. D. Shikhmurzaev, Physica D **217**, 121 (2006).
[19] Y. D. Shikhmurzaev, *Capillary Flows with Forming Interfaces* (Taylor & Francis, London, 2007).
[20] Y. D. Shikhmurzaev, Phys. Fluids **9**, 266 (1997).
[21] Y. D. Shikhmurzaev, Phys. Lett. A **245**, 378 (2005).
[22] Y. D. Shikhmurzaev, IMA J. Appl. Math. **70**, 880 (2005).
[23] Y. D. Shikhmurzaev, C. R. Mec. **333**, 205 (2005).
[24] G. I. Barenblatt and G. G. Chernyi, PMM **25**, 784 (1963).
[25] T. Qian, X.-P. Wang, and P. Sheng, J. Fluid Mech. **564**, 333 (2006).
[26] T. D. Blake and Y. D. Shikhmurzaev, J. Colloid Interface Sci. **253**, 196 (2002).
[27] W-T. Tsai and D. K. P. Yue, Annu. Rev. Fluid Mech. **28**, 249 (1996).
[28] A. V. Lukyanov, Y. D. Shikhmurzaev, and A. C. King, IMA J. Appl. Math. (to be published).